

A Theoretical Study on NO_x Selective Catalytic Reduction on single Cu-sites and Brønsted acid sites in Cu-SSZ-13

Tiago J. Goncalves,[†] Philipp N. Plessow,^{*,†} and Felix Studt^{†,‡}

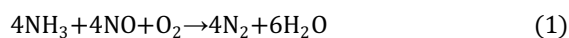
[†]Institute of Catalysis Research and Technology, Karlsruhe Institute of Technology, Hermann-von-Helmholtz Platz 1, 76344 Eggenstein-Leopoldshafen, Germany

[‡]Institute for Chemical Technology and Polymer Chemistry, Karlsruhe Institute of Technology, Engesserstrasse 18, 76131 Karlsruhe, Germany

ABSTRACT: The mechanism for Cu-SSZ-13 catalyzed Selective Catalytic Reduction (SCR) of NO_x with NH₃ is investigated for single Cu-sites. Barriers are determined for all elementary steps and are calculated with high accuracy using DLPNO-CCSD(T) single point calculations on large 46T cluster models derived from periodic density functional theory (DFT) calculations. For standard SCR, NO oxidation to NO₂ is necessary, which requires barriers above 250 kJ/mol on single Cu sites, indicating that they are not catalytically active for this process. Contrary, for fast SCR, barriers are below 150 kJ/mol, indicating that single Cu sites are active. Most of the elementary reactions, such as the required N-N bond formation between NO and NH₃ take place on the single Cu sites. After N-N bond formation, which yields H₂NNO, however, the intermediate is most easily decomposed into N₂ and H₂O on a Brønsted acid site.

INTRODUCTION

NO_x exhaust gases, products of the oxidation of nitrogen during the combustion of fuels at high temperatures, are still one of the major contributors to local air pollution, hence their emission is being strictly controlled.¹⁻² One successful strategy of reducing NO_x emissions is through their selective reduction by ammonia to N₂ over heterogeneous catalysts such as transition-metal exchanged zeolites and transition-metal oxide.³⁻²⁴ Copper-exchanged zeolites, and in particular Cu-SSZ-13, have been commercialized as they are highly active and also stable at a broad range of temperatures.^{4-6, 8, 11, 25} For that reason, the selective catalytic reduction (SCR) of ammonia over Cu-SSZ-13 has been the subject of many experimental^{4-8, 10-11, 14-15, 25-33} and theoretical studies.^{7-8, 10, 14-15, 32, 34-36} These studies led to the establishment of equations 1-3 for the reduction of NO and NO₂ to N₂.



The so-called "Standard SCR"^{3, 8, 37} is given by Equation 1. Additionally, if NO₂ is present in the exhaust gases, nitrogen can also be formed via Equation 2. This reaction is also called "Fast SCR" since its efficiency, above 473 K, is at least 10 times higher than that of the "Standard SCR".^{8, 38-39} NO₂ can be formed through the so-called "NO activation cycle" shown in Equation 3. During the standard SCR, there is no excess of NO₂ and as the fast cycle depends crucially on the availability of NO₂, the standard SCR is limited by the rate of NO₂ formation. One of the most detailed computational studies of the reaction mechanism of the standard and fast-

SCR has been reported by Janssens et al.,⁸ who proposed a consistent reaction scheme for Cu-SSZ-13. However, most of the elementary reaction steps put forward have not been investigated in detail with respect to the actual reaction barriers of the elementary reactions. Recently, Grönbeck and co-workers presented a detailed DFT-investigation, including Cu-dimers and Brønsted acid sites as active site motifs.³⁴ In addition, ammonia-SCR has so far only been investigated using density functional theory (DFT), where in addition to GGA, also DFT+U³⁴ and hybrid functionals^{10, 14, 40} have been employed. We recently found that calculations at the generalized gradient approximation (GGA) level of theory are problematic for the description of ammonia-SCR in Cu-SSZ-13 leading to errors of adsorption energies and reaction energetics of about 50 kJ/mol when compared to CCSD(T) calculations.⁴¹

In this work we investigate both, the standard and fast-SCR over single-site Cu-SSZ-13 and H-SSZ-13 using a hierarchical cluster model that allows us to obtain highly accurate reaction energies and barriers using ab initio methods.

RESULTS AND DISCUSSION

We investigate SCR on Cu-SSZ-13, focusing on the reactivity introduced by isolated Al-substitution of Si-atoms. In our computational models, we employ a unit cell containing 36 tetrahedral atoms out of which one is substituted by Al, giving a Si/Al-ratio of 35. When the introduced charge is balanced by Cu⁺, this leads to isolated, Cu-monomers as active sites (see Fig. 1a and Fig. 1b). It is also known that some of the Al-substituted sites remain charge-balanced with a proton as Brønsted acid sites (BAS).

We will study both cases separately, with only one of these active sites per unit cell.

All zeolite structures were fully optimized using dispersion-corrected DFT, specifically PBE-D3 with periodic boundary conditions (PBC). Due to the known limitations of DFT calculations at the generalized gradient approximation level of theory, ab initio calculations were additionally performed. Inspired by the work of Sauer and coworkers⁴²⁻⁴⁶ we have cut nonperiodic, large 46T cluster models (including 46 tetrahedral atoms) on which we performed additional calculations (see Fig. 1c).⁴²⁻⁵¹ The corrected energies were computed as:

$$E_{\text{CCSD(T)}}^{\text{PBC}} = E_{\text{PBE-D3}}^{\text{PBC}} + E_{\text{DLPNO-CCSD(T)}}^{46\text{T}} - E_{\text{PBE-D3}}^{46\text{T}} \quad (4)$$

Where $E_{\text{PBE-D3}}^{\text{PBC}}$ is the DFT energy obtained for the periodic model and $E_{\text{DLPNO-CCSD(T)}}^{46\text{T}}$ and $E_{\text{PBE-D3}}^{46\text{T}}$ are the energies obtained for the 46T model with DLPNO-CCSD(T) and PBE-D3, respectively. Gibbs free energies were computed based on the harmonic oscillator approximation and, for gas phase species, using additionally the rigid-rotator free translator approximation. All reported Gibbs free energies are at 473 K and 1 bar reference pressure.

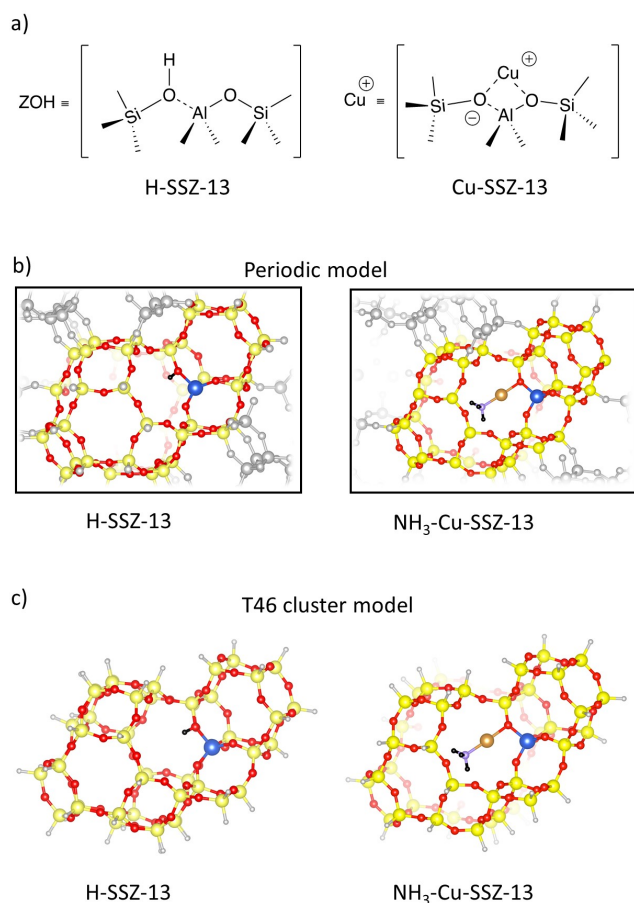


Figure 1. a) Representation of H-SSZ-13 and the Cu-SSZ-13 resonance structures. Illustration of b) the periodic model and c) the 46T cluster model for the H-SSZ-13 and Cu-SSZ-13 zeolite. Color scheme: Cu – Brown; Al – Blue; O – Red; Si – Yellow; N – Purple; H – Black; Periodic/Cluster termination – Gray.

We have investigated the mechanism of the fast SCR cycle on H/Cu-SSZ-13 starting from the mechanistic proposal

Janssens et al.⁸ The most favorable investigated path is depicted in Fig. 2a.

Before discussing the elementary steps in detail, we will first focus on particularly stable intermediates that are likely resting states of the catalytic cycle. The stability is discussed based on Gibbs free energies at 200 °C and 1 bar reference pressure. Starting from a copper site with ammonia (structure 1, according to Figure 2a) as illustrated in Fig. 1, several stable structures can be formed through adsorption. While the clean Cu atom in oxidation state 1 is most stable when located in the six-membered ring by 39 kJ/mol, when bound to adsorbates it is located in the 8-membered ring as shown in Figure 1b, which is in agreement with previous work.^{8, 52-54} We nevertheless computed the free energy for structure 5 from Fig. 2a for Cu in the 8- rather than the 6-membered ring, since we do not need to consider potential barriers for rearrangement of Cu between the two positions and because the difference in stability is eventually unimportant as both structures are high-energy intermediates. We find that both NO₂ and NH₃ adsorb strongly with adsorption free energies of -75 and -105 kJ/mol respectively. The co-adsorption of NO₂ and NH₃ is also only slightly less favorable (-100 kJ/mol). Adsorption of other potential adsorbates is significantly weaker (H₂O: -45 kJ/mol; NO: -14 kJ/mol; O₂: 3 kJ/mol; N₂: -18 kJ/mol; H₂NNO: -39 kJ/mol and HNO₂: -29 kJ/mol). The adsorption of multiple ammonia molecules leading to Cu(NH₃)_n⁺ complexes^{8, 10, 55-56} was also investigated. We note that upon adsorption of two or more ammonia molecules the formed copper complex detaches from the zeolite framework and is mobile.^{10, 15, 40, 57-59} We find free energies of -114 and -111 kJ/mol for two and three NH₃ adsorbed molecules, respectively (see Table S2). We thus find that adsorption of a second molecule of NH₃ is only 9 kJ/mol more stable. We note that Paolucci et al. have computed Cu(NH₃)₂⁺ to be more than 30 kJ/mol more stable than Cu(NH₃)₁⁺ in terms of free energy at 200 °C.⁴⁰ With an increasing number of NH₃-ligands, the Cu(NH₃)_n⁺ complex is exceedingly weakly bound to the zeolite framework and thus becomes mobile at elevated temperatures.^{15, 26, 34, 40, 60-61} This situation is poorly described by the harmonic approximation, which can to some extent be circumvented using MD simulations or approximations to the entropies of weakly bound adsorbates.³⁴ Here, we will focus on the reactivity of Cu with only a single NH₃ adsorbed and the free energy profile in Fig. 2b) is referenced to that.

The computed Gibbs free energies employing DLPNO-CCSD(T) are compared with DFT results in Table S1. In agreement with previous work,⁴¹ we find large deviations for PBE-D3, in some cases more than 50 kJ/mol. We also compare with HSE-06-TSvdw results of Paolucci and co-workers,⁴⁰ which are in most cases in very good agreement with DLPNO-CCSD(T), with deviations below 15 kJ/mol. Larger differences are observed for the mobile species Cu(NH₃)₂⁺ and Cu(NH₃)₃⁺, where the free energies computed by Paolucci and co-workers are lower by up to 40 kJ/mol. This can at least partially be attributed to the harmonic approximation applied to the motion of the nuclei in this work.

The formation of N₂ and H₂O from NO, NO₂ and NH₃ in the fast SCR-cycle requires three types of reactions: 1) transferring H from N to O, 2) N-O bond cleavage and 3) N-N bond formation. These steps can in principle occur in

different order and the path depicted in Fig. 2a is the most favorable of those that we have studied.

Starting in cycle II with Cu-NH₃ (structure 1), co-adsorption of NO₂ and a hydrogen transfer leads to an adsorbed amide (NH₂) plus nitrous acid (HNO₂), which is desorbed and released into the gas phase. This hydrogen-transfer oxidizes Cu from oxidation state +1 to +2 and is also computed to be the step with the highest barrier (143 kJ/mol) of the fast SCR. We note that nitrous acid has also been considered in previous theoretical and experimental studies but is hard to detect in reaction conditions as it is a reactive intermediate.^{11, 15, 34, 60, 62-68} Before discussing the fate of nitrous acid, we will continue with Cu-NH₂ (structure 3, cycle II in Fig. 2a). Co-adsorption of NO results in spontaneous N-N bond formation without energetic barriers, leading to side-on adsorbed H₂NNO (structure 4), which returns Cu to oxidation state +1. Overall, the formation of H₂NNO and nitrous acid (HNO₂) from NO, NO₂ and NH₃ are relatively thermoneutral reactions with a free

energy difference of -3 kJ/mol (from 1 to 1', see cycle II from Fig. 2b).

The decomposition of H₂NNO yields N₂ and H₂O and this is shown in cycle I of Fig. 2a. In agreement with previous work, we find that this reaction is most likely to occur on a Brønsted acid site rather than a Cu active site.^{4, 14, 34, 69-71} Since ammonia binds strongly to the acid site at 200 °C, we start with the ammonium cation on a Brønsted acid site (structure A, cycle I). Hydrogen transfer of H₂NNO, catalyzed by the ammonium ion, leads to double-bond formation between the nitrogen atoms, creating the HN=NOH molecule. An additional hydrogen transfer leads to the simultaneous formation of H₂O and N₂, accompanied by a large gain in free energy of around 230 kJ/mol (structure D to E, depicted in cycle I from Fig. 2a). Both N₂ and H₂O are relatively weakly bound and readily desorb to close cycle I. This cycle is expected to be the fastest, having barriers lower than 100 kJ/mol.

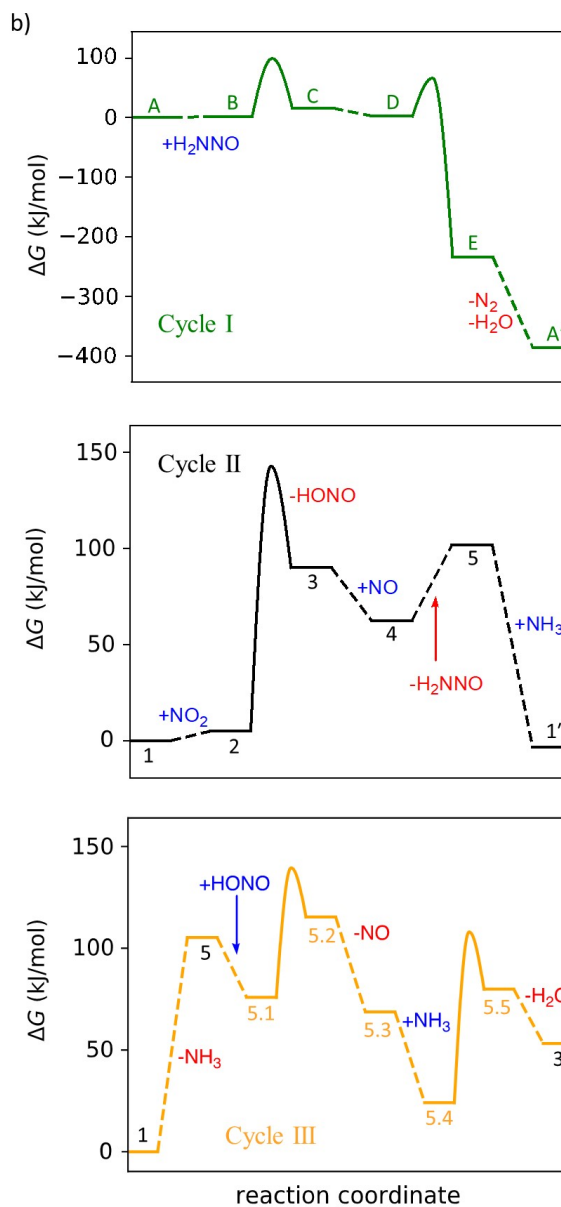
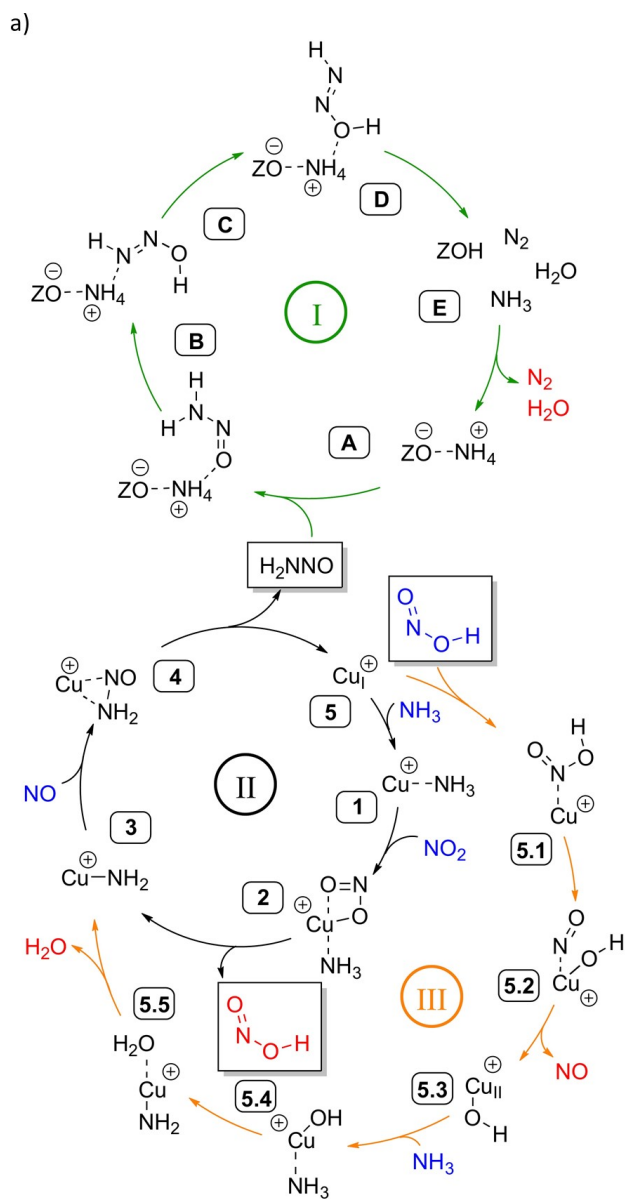


Figure 2. a) Overview of the mechanism investigated for the fast SCR cycle for catalytic conversion of NO_x into H_2O and N_2 . The redox active site is abbreviated as “Cu+” (see Fig. 1a). The mechanism is split into three cycles, where the first (I) corresponds to the decomposition of H_2NNO released during cycle II, the second (II) additionally generates nitrous acid (HNO_2) that can further react on any free Cu^+ active site (cycle III). b) Gibbs free energy profiles at 473 K of cycles I, II and III are depicted in a). The resting state ($\Delta G = 0$) is taken to be ZOH-NH_3 for cycles I and Cu-NH_3 for cycles II and III.

We now return to nitrous acid (HNO_2), which was a byproduct of cycle II. HNO_2 can further react as shown in cycle III of Fig. 2a. The reaction requires a free Cu active site that is not necessarily the same active site on which nitrous acid is formed and released in step 2-3. Since nitrous acid is a relatively small molecule and is expected to be able to diffuse through the pores of SSZ-13 it could also react at a different active site. After adsorption to form $\text{Cu-NO}_2\text{H}$ (structure 5.1), a barrier of 139 kJ/mol is required to cleave a N-O bond. This results in the formation of a separate OH and NO ligands bound to the same Cu-atom, which oxidizes Cu to oxidation state +2. NO is then readily released into the gas phase. The remaining Cu-OH (structure 5.3) can then react under co-adsorption of NH_3 , with subsequent proton transfer forming free H_2O and an amide (Cu-NH_2). Cu-NH_2 (structure 3) can then react with NO, as described above in cycle II.

Examples of transition states for each cycle depicted in Figure 2a are illustrated in Figure 3. In Figure 3a, one of the two transition states from cycle I is shown, where a hydrogen transfer between the ammonium ion and NOH_2 will simultaneously form N_2 , H_2O and NH_3 , while a proton is transferred to a different oxygen atom of the zeolite. Figure 3b and c show the rate-determining steps in cycles II and III, in which b) shows the hydrogen transfer between NH_3 and NO_2 and c) shows the N-O bond cleavage from HNO_2 .

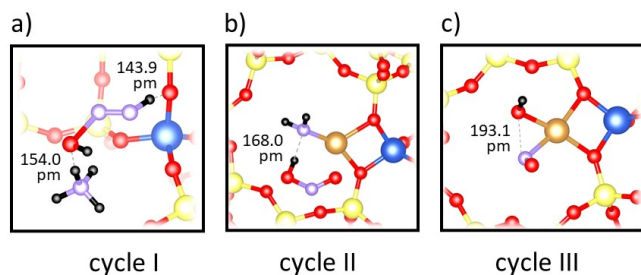


Figure 3. Structure of important transition states for cycle I, II and III. a) Concerted decomposition of H_2NNOH into molecular N_2 and H_2O , TS(D-E) . b) Proton transfer between NH_3 and NO_2 and subsequent nitrous acid desorption, TS(2-3) . c) Dissociation of nitrous acid into copper-adsorbed nitric oxide and hydroxide, TS(5.1-5.2) . Color scheme: Cu – Brown; Al – Blue; O – Red; Si – Yellow; H – Black; N – Purple.

Figure 2 b) shows the free energy profiles for cycles I, II and III depicted in Fig. 2a). We find that barriers are in a reasonable range, with the highest barrier for step 2-3, which is 143 kJ/mol (Fig 3b). The barrier for decomposition of nitric acid in step 5.1-5.2 is similar (139 kJ/mol, Fig 3c), while the decomposition of H_2NNO on the BAS, clearly required the lowest barriers (<100 kJ/mol). A quantitative analysis of the activity of the catalyst will of course require the use of microkinetic modelling using the actual partial pressures of NO_x and NH_3 . Based on the free energy diagrams for cycle II and III shown in Fig.2c), it is clear that $\text{Cu(NH}_3)_n^+$ is computed to be the most stable state and likely the resting state of the catalytic cycle. For most other states, no significant coverage is expected.

We have additionally studied standard SCR on single Cu active site and the investigated mechanism is shown in Fig 3a. Starting from a clean Cu-site (structure 5), adsorption of O_2 leads first to the formation of side-on bound oxygen. After rearrangement of the adsorbed O_2 and co-adsorption of NO (structure 5c), oxidation of NO leads to coadsorbed NO_2 and O (structure 5e). It is worth mentioning that 5e can rearrange with relatively low barriers to η^1 - and η^2 -bound nitrate (structures 5 α and 5 β), having free energies of 46 and -21 kJ/mol with respect to Cu-NH_3 . Adsorption and oxidation of a second NO molecule leads to two coadsorbed NO_2 molecules, which are then desorbed to recover the active site. The involved barriers are a clearly too high for this cycle to be active (>250 kJ/mol) (see Fig. 4), at least for the mechanism investigated in this work. This agrees with previous investigations that propose that Cu-dimers are required for NO-activation.^{8, 10, 15, 55, 61, 72-76}

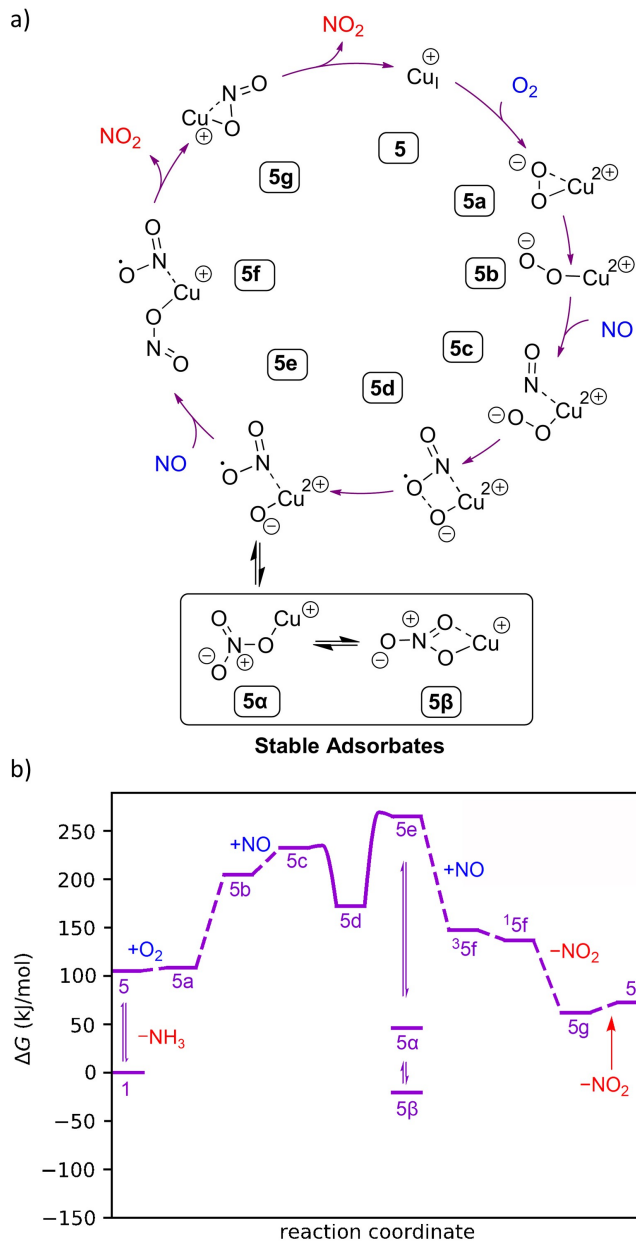


Figure 4. a) Investigated NO activation cycle. b) Gibbs free energy profile at 473 K of the cycle depicted in a). Barriers with entropy corrections that result in slightly lower free energies (5c-5d) than their minima are raised to 5 kJ/mol. ^{35f} and ^{15f} are triplet and singlet states of structure “5f”. The resting state is considered to be Cu-NH₃ ($\Delta G = 0$). Intrinsic reaction barriers between “5e”, “5 α ” and “5 β ” are low and are hence omitted for clarity.

A Bader charge analysis was performed based on the electron density computed with PBE-D3 for periodic structures to analyze the oxidation state of copper during the reaction cycles II, III and NO oxidation (see Fig. 5a). Cu^I and Cu^{II} ranges are defined based on Bader charges of structures 5 (Cu^I) and 5.3 (Cu^{II}-OH), to which one can very clearly assign oxidation states.^{8, 14, 77} Copper Bader charges closer to structure 5 (+0.72 *e*) are then considered to have an oxidation state of +1, while Bader charges closer to structure 5.3 (+1.0 *e*) are considered to have an oxidation state of +2, which is in line with ref.⁵⁵

The assignment of the oxidation states of copper based on Bader charges within cycle II agrees with the formal

oxidation states assigned based on Fig. 2a, although the Bader charge of the amide Cu-NH₂ is on the border between oxidation state +1 and +2. The oxidation state change in cycle III, where Cu is oxidized through the formation of an OH-ligand (structure 5.2) is also well reproduced by the Bader charge analysis. In the NO-oxidation cycle investigated in Fig. 3, Cu is in oxidation state +2, except in the initial state and this is again well-reproduced by the Bader charges in Fig 5b.

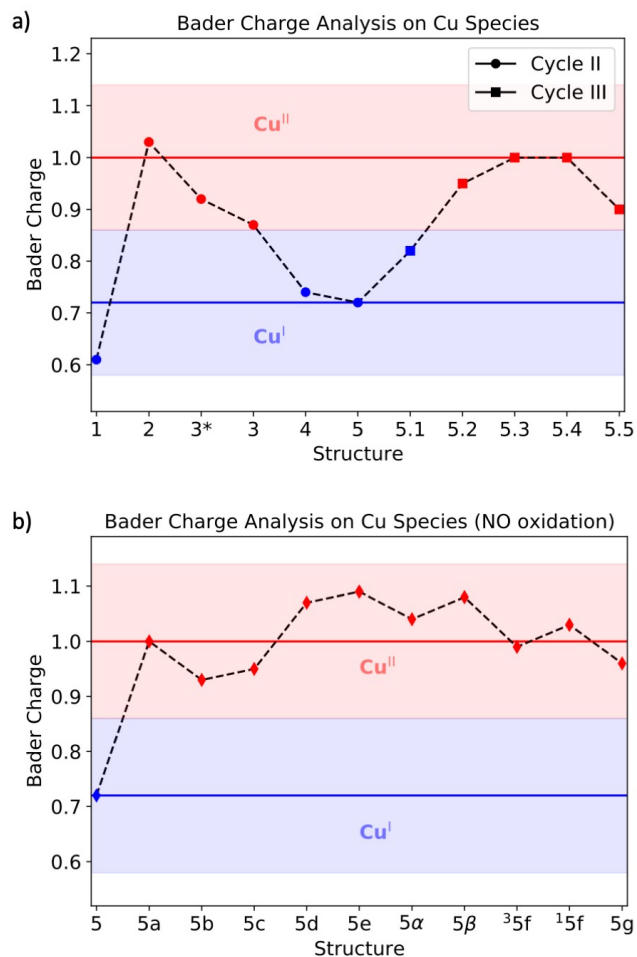


Figure 5. Bader charge analysis on copper species from a) cycle II/III and b) NO oxidation, referenced to structure 5 (Cu^I) and structure 5.3 (Cu^{II}-OH), which have known oxidation states.^{8, 14, 77} Structures are labeled according to Figure 2 a. 3* depicts structure 3 with nitrous acid desorbed but present within the cavity.

CONCLUSIONS

We have investigated the complete catalytic cycle for the Selective Catalytic Reduction (SCR) of NO_x with NH₃ catalyzed by single Cu-sites in Cu-exchanged SSZ-13 and Brønsted acid sites. Periodic DFT calculations were supplemented with highly accurate DLPNO-CCSD(T) calculations on cluster models.

We find reasonably low free energy barriers (< 150 kJ/mol) for the fast SCR cycle in which NO and NO₂ are

available in equal amounts. The highest computed barrier (143 kJ/mol) occurs for nitrous acid (HNO₂) formation, which involves a hydrogen transfer from ammonia to nitrogen dioxide. The decomposition of nitrous acid, which requires N-O bond cleavage requires a similar barrier (139 kJ/mol). Reactions occurring on Brønsted acid sites mainly involve hydrogen transfer reaction and only require low barriers (< 100 kJ/mol). For standard SCR, we find insurmountable barriers of > 250 kJ/mol for the investigated mechanism for the NO oxidation with single copper sites, strongly suggesting that the reaction needs different active site motifs.

METHODS

Periodic DFT calculations were carried out using the VASP program package⁷⁸⁻⁸² with the PAW method^{78, 82} and the PBE-D3 functional to find minima and transition states. TS scans were performed with constrained optimizations using ARPES⁸³. The dimer method⁸⁴ and Nudged Elastic Band⁸⁵⁻⁸⁸ from the Atomic Simulation Environment⁸⁹ were also used.

To improve the reaction energies and barriers, a cluster is cut from the periodic structure, so that the entire cavity from the Cu-SSZ-13 is modelled and the H-terminations are at least five bonds away from the active site, containing 46 tetrahedral atoms. DLPNO-CCSD(T)/def2-TZVPP⁵⁰⁻⁵¹ single-point calculations were then performed with the Quasi-Restricted Orbital⁹⁰ treatment using the ORCA program package⁹⁰⁻⁹¹ as well as PBE-D3 with TURBOMOLE.⁹²⁻⁹³ Energies were then computed according to Eq. 4. For calculations on the BAS, H-SSZ-13, we employ DLPNO-CCSD(T)/cc-pVDZ calculations along with CBS-extrapolation using DLPNO-MP2/cc-pVXZ calculations. Here we extrapolate the correlation energy using the 2-point l^{-3} formula⁹⁴ with $X=2,3$ and the Hartree-Fock energy with the 3-point exponential formula⁹⁵ and $X=2,3,4$.

Harmonic frequencies were computed based on a partial Hessian computed with finite differences in which all adsorbate atoms and only the (Si-O)₄-Al fragment of the zeolite at the active site was considered.

We have evaluated D1 diagnostics on the canonical CCSD/def2-TZVPP⁹⁶⁻¹⁰⁰ level of theory for T1 cluster models to check how reliable single-reference coupled-cluster results are. The T1 cluster models were optimized at the PBE-D3/dhf-SV(P)^{96-97, 101-105} level of theory using the RI approximation¹⁰⁶. All calculations on T1 clusters were performed with the TURBOMOLE program package.⁹²⁻⁹³ Table S3 from the SI shows D1 diagnostics for the structures used in this work. Additionally, we compared DLPNO-CCSD(T) with DLPNO-CCSD to see the contribution of perturbative triples in reaction energies and transition states for the 46T cluster models (Table S4 from the SI). Structures and barriers that may indicate multi-reference character for the fast SCR (cycles II and III) are 4, 5.2 and TS_5.1-5.2 with D1 diagnostics of 0.19, 0.19 and 0.18 respectively which, according to ref.¹⁰⁰, already indicates multi-reference character (values above 0.15 for catalysts with transition metals). Also, adding perturbative triple excitations on total energies result in reaction energy changes below 30 kJ/mol except for structure 5.2, with a 55

kJ/mol difference with respect to the CCSD reaction energy ($\Delta E_{CCSD(T)}$ being lower). The NO oxidation cycle, on the other hand, contains several structures with a strong multi-reference character, with D1 diagnostics between 0.2 and 0.3 and perturbative triple excitations resulting in reaction energy changes between 32 and 92 kJ/mol, leading to less reliable results, see Tables S3 and S6. Likewise, spin contamination is much larger in UHF orbitals for the NO oxidation cycle, see Figures S5-S7. Nevertheless, it is clear that the overall barriers for NO oxidation are very high (above 200 kJ/mol) as the free energy barrier for the RDS is 271 kJ/mol with the M06 functional¹⁰⁷ (see SI) and 169 kJ/mol with PBE-D3, which is known for underestimating transition states.^{41, 44}

The coordinates of all structures used in this work are available in the supporting information.

ASSOCIATED CONTENT

Supporting Information

The Supporting Information is available free of charge on the ACS Publications website.

Computed energies, further analysis and Cartesian coordinates (PDF).

AUTHOR INFORMATION

Corresponding Author

* E-mail: plessow@kit.edu

Notes

The authors declare no competing financial interest.

ACKNOWLEDGMENT

The authors acknowledge support by the state of Baden-Württemberg through bwHPC (bwunicluster and JUSTUS, RV bw17D011). Financial support from the Helmholtz Association is also gratefully acknowledged.

REFERENCES

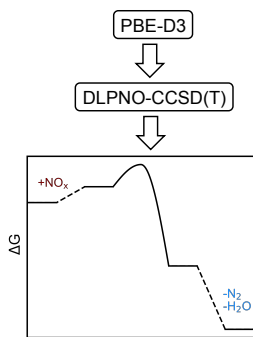
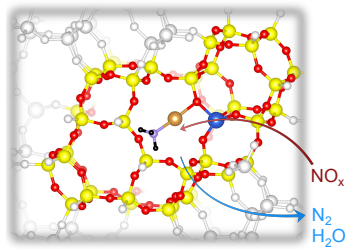
1. Ciardelli, C.; Nova, I.; Tronconi, E.; Chatterjee, D.; Bandl-Konrad, B.; Weibel, M.; Krutzsch, B., Reactivity of NO/NO₂-NH₃ SCR system for diesel exhaust aftertreatment: Identification of the reaction network as a function of temperature and NO₂ feed content. *Appl. Catal. B* **2007**, *70*, 80-90.
2. Rahkamaa-Tolonen, K.; Maunula, T.; Lomma, M.; Huuhtanen, M.; Keiski, R. L., The effect of NO₂ on the activity of fresh and aged zeolite catalysts in the NH₃-SCR reaction. *Catal. Today* **2005**, *100*, 217-222.
3. Kato, A.; Matsuda, S.; Kamo, T.; Nakajima, F.; Kuroda, H.; Narita, T., Reaction between nitrogen oxide (NO_x) and ammonia on iron oxide-titanium oxide catalyst. *J. Phys. Chem.* **1981**, *85*, 4099-4102.
4. Beale, A. M.; Gao, F.; Lezcano-Gonzalez, I.; Peden, C. H.; Szanyi, J., Recent advances in automotive catalysis for NO_x emission control by small-pore microporous materials. *Chem. Soc. Rev.* **2015**, *44*, 7371-7405.

5. Lomachenko, K. A.; Borfecchia, E.; Negri, C.; Berlier, G.; Lamberti, C.; Beato, P.; Falsig, H.; Bordiga, S., The Cu-CHA deNOx catalyst in action: temperature-dependent NH₃-assisted selective catalytic reduction monitored by operando XAS and XES. *J. Am. Chem. Soc.* **2016**, *138*, 12025-12028.
6. Bates, S. A.; Verma, A. A.; Paolucci, C.; Parekh, A. A.; Anggara, T.; Yezerets, A.; Schneider, W. F.; Miller, J. T.; Delgass, W. N.; Ribeiro, F. H., Identification of the active Cu site in standard selective catalytic reduction with ammonia on Cu-SSZ-13. *J. Catal.* **2014**, *312*, 87-97.
7. McEwen, J.-S.; Anggara, T.; Schneider, W.; Kispersky, V.; Miller, J.; Delgass, W.; Ribeiro, F., Integrated operando X-ray absorption and DFT characterization of Cu-SSZ-13 exchange sites during the selective catalytic reduction of NOx with NH₃. *Catal. Today* **2012**, *184*, 129-144.
8. Janssens, T. V.; Falsig, H.; Lundegaard, L. F.; Vennestrom, P. N.; Rasmussen, S. B.; Moses, P. G.; Giordano, F.; Borfecchia, E.; Lomachenko, K. A.; Lamberti, C., A consistent reaction scheme for the selective catalytic reduction of nitrogen oxides with ammonia. *ACS Catal.* **2015**, *5*, 2832-2845.
9. Berthomieu, D.; Delahay, G., Recent advances in Cu/IIY: experiments and modeling. *Catal. Rev.* **2006**, *48*, 269-313.
10. Paolucci, C.; Khurana, I.; Parekh, A. A.; Li, S.; Shih, A. J.; Li, H.; Di Iorio, J. R.; Albarracin-Caballero, J. D.; Yezerets, A.; Miller, J. T., Dynamic multinuclear sites formed by mobilized copper ions in NOx selective catalytic reduction. *Science* **2017**, *357*, 898-903.
11. Gao, F.; Kwak, J. H.; Szanyi, J.; Peden, C. H., Current understanding of Cu-exchanged chabazite molecular sieves for use as commercial diesel engine DeNOx catalysts. *Top. Catal.* **2013**, *56*, 1441-1459.
12. Kieger, S.; Delahay, G.; Coq, B.; Neveu, B., Selective catalytic reduction of nitric oxide by ammonia over Cu-FAU catalysts in oxygen-rich atmosphere. *J. Catal.* **1999**, *183*, 267-280.
13. Yu, T.; Hao, T.; Fan, D.; Wang, J.; Shen, M.; Li, W., Recent NH₃-SCR mechanism research over Cu/SAPO-34 catalyst. *J. Phys. Chem. C* **2014**, *118*, 6565-6575.
14. Paolucci, C.; Verma, A. A.; Bates, S. A.; Kispersky, V. F.; Miller, J. T.; Gounder, R.; Delgass, W. N.; Ribeiro, F. H.; Schneider, W. F., Isolation of the copper redox steps in the standard selective catalytic reduction on Cu-SSZ-13. *Angew. Chem. Int. Ed.* **2014**, *53*, 11828-11833.
15. Gao, F.; Mei, D.; Wang, Y.; Szanyi, J. n.; Peden, C. H., Selective catalytic reduction over Cu/SSZ-13: linking homo- and heterogeneous catalysis. *J. Am. Chem. Soc.* **2017**, *139*, 4935-4942.
16. Tajima, N.; Hashimoto, M.; Toyama, F.; El-Nahas, A. M.; Hirao, K., A theoretical study on the catalysis of Cu-exchanged zeolite for the decomposition of nitric oxide. *Phys. Chem. Chem. Phys.* **1999**, *1*, 3823-3830.
17. Brandenberger, S.; Kröcher, O.; Tissler, A.; Althoff, R., The state of the art in selective catalytic reduction of NOx by Ammonia using metal-exchanged zeolite catalysts. *Catal. Rev.* **2008**, *50*, 492-531.
18. Nova, I.; Tronconi, E., *Urea-SCR technology for deNOx after treatment of diesel exhausts*; Springer, 2014; Vol. 5.
19. Schwidder, M.; Kumar, M. S.; Bentrup, U.; Pérez-Ramírez, J.; Brückner, A.; Grünert, W., The role of Brønsted acidity in the SCR of NO over Fe-MFI catalysts. *Microporous Mesoporous Mater.* **2008**, *111*, 124-133.
20. Irfan, M. F.; Goo, J. H.; Kim, S. D., Co₃O₄ based catalysts for NO oxidation and NOx reduction in fast SCR process. *Appl. Catal. B* **2008**, *78*, 267-274.
21. Wang, D.; Zhang, L.; Kamasamudram, K.; Epling, W. S., In situ-DRIFTS study of selective catalytic reduction of NOx by NH₃ over Cu-exchanged SAPO-34. *ACS Catal.* **2013**, *3*, 871-881.
22. Kucherov, A. V.; Gerlock, J. L.; Jen, H.-W.; Shelef, M., In situ ESR monitoring of the coordination and oxidation states of copper in Cu-ZSM-5 up to 500° C in flowing gas mixtures: 1. Interaction with He, O₂, NO, NO₂, and H₂O. *Zeolites* **1995**, *15*, 9-14.
23. Bendrich, M.; Scheuer, A.; Hayes, R.; Votsmeier, M., Unified mechanistic model for Standard SCR, Fast SCR, and NO₂ SCR over a copper chabazite catalyst. *Appl. Catal. B* **2018**, *222*, 76-87.
24. Colombo, M.; Nova, I.; Tronconi, E., NO₂ adsorption on Fe- and Cu-zeolite catalysts: The effect of the catalyst red-ox state. *Appl. Catal. B* **2012**, *111*, 433-444.
25. Kwak, J. H.; Tonkyn, R. G.; Kim, D. H.; Szanyi, J.; Peden, C. H., Excellent activity and selectivity of Cu-SSZ-13 in the selective catalytic reduction of NOx with NH₃. *J. Catal.* **2010**, *275*, 187-190.
26. Marberger, A.; Petrov, A. W.; Steiger, P.; Elsener, M.; Kröcher, O.; Nachttegaal, M.; Ferri, D., Time-resolved copper speciation during selective catalytic reduction of NO on Cu-SSZ-13. *Nat. Catal.* **2018**, *1*, 221-227.
27. Leistner, K.; Kumar, A.; Kamasamudram, K.; Olsson, L., Mechanistic study of hydrothermally aged Cu/SSZ-13 catalysts for ammonia-SCR. *Catal. Today* **2018**, *307*, 55-64.
28. Ma, L.; Cheng, Y.; Cavataio, G.; McCabe, R. W.; Fu, L.; Li, J., Characterization of commercial Cu-SSZ-13 and Cu-SAPO-34 catalysts with hydrothermal treatment for NH₃-SCR of NOx in diesel exhaust. *Chem. Eng. J.* **2013**, *225*, 323-330.
29. Xie, K.; Wang, A.; Woo, J.; Kumar, A.; Kamasamudram, K.; Olsson, L., Deactivation of Cu-SSZ-13 SCR catalysts by vapor-phase phosphorus exposure. *Appl. Catal. B* **2019**, *256*, 117815.
30. Wijayanti, K.; Xie, K.; Kumar, A.; Kamasamudram, K.; Olsson, L., Effect of gas compositions on SO₂ poisoning over Cu/SSZ-13 used for NH₃-SCR. *Appl. Catal. B* **2017**, *219*, 142-154.
31. Liu, L.; Wu, X.; Ma, Y.; Zhang, X.; Ran, R.; Si, Z.; Weng, D., Potassium deactivation of Cu-SSZ-13 catalyst for NH₃-SCR: Evolution of salts, zeolite and copper species. *Chem. Eng. J.* **2020**, *383*, 123080.
32. Tyrsted, C.; Borfecchia, E.; Berlier, G.; Lomachenko, K.; Lamberti, C.; Bordiga, S.; Vennestrom, P.; Janssens, T.; Falsig, H.; Beato, P., Nitrate-nitrite equilibrium in the reaction of NO with a Cu-CHA catalyst for NH₃-SCR. *Catal. Sci. Technol.* **2016**, *6*, 8314-8324.
33. Andersen, C. W.; Borfecchia, E.; Bremholm, M.; Jørgensen, M. R. V.; Vennestrom, P. N. R.; Lamberti, C.; Lundegaard, L. F.; Iversen, B. B., Redox-Driven Migration of Copper Ions in the Cu-CHA Zeolite as Shown by the In Situ PXRD/XANES Technique. *Angew. Chem.* **2017**, *129*, 10503-10508.
34. Chen, L.; Janssens, T. V.; Vennestrom, P. N.; Jansson, J.; Skoglundh, M.; Grönbeck, H., A Complete Multisite Reaction Mechanism for Low-Temperature NH₃-SCR over Cu-CHA. *ACS Catal.* **2020**, *10*, 5646-5656.
35. Zhao, P.; Boekfa, B.; Shimizu, K.-i.; Ogura, M.; Ehara, M., Selective catalytic reduction of NO with NH₃ over Cu-exchanged CHA, GME, and AFX zeolites: a density functional theory study. *Catal. Sci. Technol.* **2021**.
36. Moreno-González, M.; Millán, R.; Concepción, P.; Blasco, T.; Boronat, M., Spectroscopic Evidence and Density Functional Theory (DFT) Analysis of Low-Temperature Oxidation of Cu+ to Cu²⁺ NOx in Cu-CHA Catalysts: Implications for the SCR-NOx Reaction Mechanism. *ACS Catal.* **2019**, *9*, 2725-2738.
37. Arnarson, L.; Falsig, H.; Rasmussen, S. B.; Lauritsen, J. V.; Moses, P. G., A complete reaction mechanism for standard and fast selective catalytic reduction of nitrogen oxides on low coverage VOx/TiO₂ (0 0 1) catalysts. *J. Catal.* **2017**, *346*, 188-197.
38. Han, L.; Cai, S.; Gao, M.; Hasegawa, J.-y.; Wang, P.; Zhang, J.; Shi, L.; Zhang, D., Selective Catalytic Reduction of NOx with NH₃ by Using Novel Catalysts: State of the Art and Future Prospects. *Chem. Rev.* **2019**, *119*, 10916-10976.
39. Koebel, M.; Elsener, M.; Madia, G., Reaction pathways in the selective catalytic reduction process with NO and NO₂ at low temperatures. *Ind. Eng. Chem. Res.* **2001**, *40*, 52-59.

40. Paolucci, C.; Parekh, A. A.; Khurana, I.; Di Iorio, J. R.; Li, H.; Albarracin Caballero, J. D.; Shih, A. J.; Anggara, T.; Delgass, W. N.; Miller, J. T., Catalysis in a cage: condition-dependent speciation and dynamics of exchanged Cu cations in SSZ-13 zeolites. *J. Am. Chem. Soc.* **2016**, *138*, 6028-6048.
41. Goncalves, T. J.; Plessow, P. N.; Studt, F., On the Accuracy of Density Functional Theory in Zeolite Catalysis. *ChemCatChem* **2019**, *11*, 4368-4376.
42. Tuma, C.; Kerber, T.; Sauer, J., The tert-Butyl Cation in H-Zeolites: Deprotonation to Isobutene and Conversion into Surface Alkoxides. *Angew. Chem. Int. Ed.* **2010**, *49*, 4678-4680.
43. Tuma, C.; Sauer, J., Treating dispersion effects in extended systems by hybrid MP2: DFT calculations—protonation of isobutene in zeolite ferrierite. *Phys. Chem. Chem. Phys.* **2006**, *8*, 3955-3965.
44. Hansen, N.; Kerber, T.; Sauer, J.; Bell, A. T.; Keil, F. J., Quantum chemical modeling of benzene ethylation over H-ZSM-5 approaching chemical accuracy: a hybrid MP2: DFT study. *J. Am. Chem. Soc.* **2010**, *132*, 11525-11538.
45. Svelle, S.; Tuma, C.; Rozanska, X.; Kerber, T.; Sauer, J., Quantum chemical modeling of zeolite-catalyzed methylation reactions: toward chemical accuracy for barriers. *J. Am. Chem. Soc.* **2009**, *131*, 816-825.
46. Rybicki, M.; Sauer, J., Ab Initio Prediction of Proton Exchange Barriers for Alkanes at Brønsted Sites of Zeolite H-MFI. *J. Am. Chem. Soc.* **2018**, *140*, 18151-18161.
47. Plessow, P. N.; Studt, F., Olefin methylation and cracking reactions in H-SSZ-13 investigated with ab initio and DFT calculations. *Catal. Sci. Technol.* **2018**, *8*, 4420-4429.
48. Plessow, P. N.; Studt, F., Unraveling the mechanism of the initiation reaction of the methanol to olefins process using ab initio and DFT calculations. *ACS Catal.* **2017**, *7*, 7987-7994.
49. Keil, F. J., Molecular modelling for reactor design. *Annu. Rev. Chem. Biomol. Eng.* **2018**, *9*, 201-227.
50. Minenkov, Y.; Chermak, E.; Cavallo, L., Accuracy of DLPNO-CCSD(T) method for noncovalent bond dissociation enthalpies from coinage metal cation complexes. *J. Chem. Theory Comput.* **2015**, *11*, 4664-4676.
51. Minenkov, Y.; Bistoni, G.; Riplinger, C.; Auer, A. A.; Neese, F.; Cavallo, L., Pair natural orbital and canonical coupled cluster reaction enthalpies involving light to heavy alkali and alkaline earth metals: the importance of sub-valence correlation. *Phys. Chem. Chem. Phys.* **2017**, *19*, 9374-9391.
52. Uzunova, E. L.; Mikosch, H.; St. Nikolov, G., Density functional study of copper-exchanged zeolites and related microporous materials: Adsorption of nitrosyls. *Int. J. Quantum Chem.* **2013**, *113*, 723-728.
53. Szanyi, J.; Kwak, J. H.; Zhu, H.; Peden, C. H., Characterization of Cu-SSZ-13 NH₃ SCR catalysts: an in situ FTIR study. *Phys. Chem. Chem. Phys.* **2013**, *15*, 2368-2380.
54. Zhang, R.; McEwen, J.-S.; Kollár, M. r.; Gao, F.; Wang, Y.; Szanyi, J.; Peden, C. H., NO chemisorption on Cu/SSZ-13: a comparative study from infrared spectroscopy and DFT calculations. *ACS Catal.* **2014**, *4*, 4093-4105.
55. Chen, L.; Janssens, T. V.; Grönbeck, H., A comparative test of different density functionals for calculations of NH₃-SCR over Cu-Chabazite. *Phys. Chem. Chem. Phys.* **2019**, *21*, 10923-10930.
56. Anggara, T.; Paolucci, C.; Schneider, W. F., Periodic DFT Characterization of NO_x Adsorption in Cu-Exchanged SSZ-13 Zeolite Catalysts. *J. Phys. Chem. C* **2016**, *120*, 27934-27943.
57. Rizzotto, V.; Chen, P.; Simon, U., Mobility of NH₃-solvated CuII ions in Cu-SSZ-13 and Cu-ZSM-5 NH₃-SCR catalysts: a comparative impedance spectroscopy study. *Catalysts* **2018**, *8*, 162.
58. Millan, R.; Cnudde, P.; Hoffman, A. E.; Lopes, C. W.; Concepción, P.; Van Speybroeck, V.; Boronat, M., Theoretical and Spectroscopic Evidence of the Dynamic Nature of Copper Active Sites in Cu-CHA Catalysts under Selective Catalytic Reduction (NH₃-SCR-NO_x) Conditions. *J. Phys. Chem. Lett.* **2020**, *11*, 10060-10066.
59. Göttl, F.; Sautet, P.; Hermans, I., Can Dynamics Be Responsible for the Complex Multiplex Infrared Spectra of NO Adsorbed to Copper (II) Sites in Zeolites? *Angew. Chem. Int. Ed.* **2015**, *54*, 7799-7804.
60. Usberti, N.; Gramigni, F.; Nasello, N. D.; Iacobone, U.; Selleri, T.; Hu, W.; Liu, S.; Gao, X.; Nova, I.; Tronconi, E., An experimental and modelling study of the reactivity of adsorbed NH₃ in the low temperature NH₃-SCR reduction half-cycle over a Cu-CHA catalyst. *Appl. Catal. B* **2020**, *279*, 119397.
61. Hu, W.; Selleri, T.; Gramigni, F.; Fenes, E.; Rout, K. R.; Liu, S.; Nova, I.; Chen, D.; Gao, X.; Tronconi, E., On the Redox Mechanism of Low-Temperature NH₃-SCR over Cu-CHA: A Combined Experimental and Theoretical Study of the Reduction Half Cycle. *Angew. Chem. Int. Ed.* **2021**, DOI: 10.1002/anie.202014926.
62. Ruggeri, M. P.; Selleri, T.; Colombo, M.; Nova, I.; Tronconi, E., Identification of nitrites/HONO as primary products of NO oxidation over Fe-ZSM-5 and their role in the Standard SCR mechanism: A chemical trapping study. *J. Catal.* **2014**, *311*, 266-270.
63. Brosius, R.; Martens, J. A., Reaction mechanisms of lean-burn hydrocarbon SCR over zeolite catalysts. *Top. Catal.* **2004**, *28*, 119-130.
64. Chen, H.-Y.; Voskoboinikov, T.; Sachtler, W. M., Reduction of NO_x over Fe/ZSM-5 catalysts: mechanistic causes of activity differences between alkanes. *Catal. Today* **1999**, *54*, 483-494.
65. Nova, I.; Ciardelli, C.; Tronconi, E.; Chatterjee, D.; Bandl-Konrad, B., NH₃-NO/NO₂ chemistry over V-based catalysts and its role in the mechanism of the Fast SCR reaction. *Catal. Today* **2006**, *114*, 3-12.
66. Ruggeri, M. P.; Grossale, A.; Nova, I.; Tronconi, E.; Jirglova, H.; Sobalik, Z., FTIR in situ mechanistic study of the NH₃NO/NO₂ "Fast SCR" reaction over a commercial Fe-ZSM-5 catalyst. *Catal. Today* **2012**, *184*, 107-114.
67. Grossale, A.; Nova, I.; Tronconi, E.; Chatterjee, D.; Weibel, M., The chemistry of the NO/NO₂-NH₃ "fast" SCR reaction over Fe-ZSM5 investigated by transient reaction analysis. *J. Catal.* **2008**, *256*, 312-322.
68. Sun, Q.; Gao, Z. X.; Chen, H. Y.; Sachtler, W. M., Reduction of NO_x with ammonia over Fe/MFI: reaction mechanism based on isotopic labeling. *J. Catal.* **2001**, *201*, 89-99.
69. Cui, Y.; Gao, F., Cu Loading Dependence of Fast NH₃-SCR on Cu/SSZ-13. *Emiss. Control Sci. Technol.* **2019**, *5*, 124-132.
70. Li, J.; Li, S., New insight into selective catalytic reduction of nitrogen oxides by ammonia over H-form zeolites: a theoretical study. *Phys. Chem. Chem. Phys.* **2007**, *9*, 3304-3311.
71. Brüggemann, T. C.; Keil, F. J., Theoretical investigation of the mechanism of the selective catalytic reduction of nitric oxide with ammonia on H-form zeolites. *J. Phys. Chem. C* **2008**, *112*, 17378-17387.
72. Chen, L.; Falsig, H.; Janssens, T. V.; Grönbeck, H., Activation of oxygen on (NH₃CuNH₃)⁺ in NH₃-SCR over Cu-CHA. *J. Catal.* **2018**, *358*, 179-186.
73. Verma, A. A.; Bates, S. A.; Anggara, T.; Paolucci, C.; Parekh, A. A.; Kamasamudram, K.; Yezerets, A.; Miller, J. T.; Delgass, W. N.; Schneider, W. F., NO oxidation: A probe reaction on Cu-SSZ-13. *J. Catal.* **2014**, *312*, 179-190.
74. Gao, F.; Washton, N. M.; Wang, Y.; Kollár, M.; Szanyi, J.; Peden, C. H., Effects of Si/Al ratio on Cu/SSZ-13 NH₃-SCR catalysts: Implications for the active Cu species and the roles of Brønsted acidity. *J. Catal.* **2015**, *331*, 25-38.
75. Falsig, H.; Vennestrom, P. N.; Moses, P. G.; Janssens, T. V., Activation of Oxygen and NO in NH₃-SCR over Cu-CHA Catalysts Evaluated by Density Functional Theory. *Top. Catal.* **2016**, *59*, 861-865.

76. Chen, L.; Janssens, T. V.; Skoglundh, M.; Grönbeck, H., Interpretation of NH₃-TPD Profiles from Cu-CHA Using First-Principles Calculations. *Top. Catal.* **2019**, *62*, 93-99.
77. Doronkin, D. E.; Casapu, M.; Günter, T.; Müller, O.; Frahm, R.; Grunwaldt, J.-D., Operando Spatially-and Time-Resolved XAS Study on Zeolite Catalysts for Selective Catalytic Reduction of NO_x by NH₃. *J. Phys. Chem. C* **2014**, *118*, 10204-10212.
78. Kresse, G.; Furthmüller, J., Efficient iterative schemes for ab initio total-energy calculations using a plane-wave basis set. *Phys. Rev. B* **1996**, *54*, 11169-11186.
79. Kresse, G.; Furthmüller, J., Efficiency of ab-initio total energy calculations for metals and semiconductors using a plane-wave basis set. *Comput. Mater. Sci.* **1996**, *6*, 15-50.
80. Kresse, G.; Hafner, J., Ab initio molecular dynamics for liquid metals. *Phys. Rev. B* **1993**, *47*, 558.
81. Kresse, G.; Hafner, J., Ab initio molecular-dynamics simulation of the liquid-metal-amorphous-semiconductor transition in germanium. *Phys. Rev. B* **1994**, *49*, 14251.
82. Kresse, G.; Joubert, D., From ultrasoft pseudopotentials to the projector augmented-wave method. *Phys. Rev. B* **1999**, *59*, 1758.
83. Plessow, P. N., Efficient transition state optimization of periodic structures through automated relaxed potential energy surface scans. *J. Chem. Theory Comput.* **2018**, *14*, 981-990.
84. Henkelman, G.; Jónsson, H., A dimer method for finding saddle points on high dimensional potential surfaces using only first derivatives. *J. Chem. Phys.* **1999**, *111*, 7010-7022.
85. Berne, B. J.; Ciccotti, G.; Coker, D. F., *Classical and Quantum Dynamics in Condensed Phase Simulations: Proceedings of the International School of Physics*; World Scientific, 1998.
86. Henkelman, G.; Jónsson, H., Improved tangent estimate in the nudged elastic band method for finding minimum energy paths and saddle points. *J. Chem. Phys.* **2000**, *113*, 9978-9985.
87. Henkelman, G.; Uberuaga, B. P.; Jónsson, H., A climbing image nudged elastic band method for finding saddle points and minimum energy paths. *J. Chem. Phys.* **2000**, *113*, 9901-9904.
88. Smidstrup, S.; Pedersen, A.; Stokbro, K.; Jónsson, H., Improved initial guess for minimum energy path calculations. *J. Chem. Phys.* **2014**, *140*, 214106.
89. Larsen, A. H.; Mortensen, J. J.; Blomqvist, J.; Castelli, I. E.; Christensen, R.; Dulak, M.; Friis, J.; Groves, M. N.; Hammer, B.; Hargus, C., The atomic simulation environment—a Python library for working with atoms. *J. Phys. Condens. Matter* **2017**, *29*, 273002.
90. Neese, F., Software update: the ORCA program system, version 4.0. *Wiley Interdiscip. Rev. Comput. Mol. Sci.* **2018**, *8*, e1327.
91. Neese, F., The ORCA program system. *Wiley Interdiscip. Rev. Comput. Mol. Sci.* **2012**, *2*, 73-78.
92. Ahlrichs, R.; Bär, M.; Häser, M.; Horn, H.; Kölmel, C., Electronic structure calculations on workstation computers: The program system turbomole. *Chem. Phys. Lett.* **1989**, *162*, 165-169.
93. Von Arnim, M.; Ahlrichs, R., Performance of parallel TURBOMOLE for density functional calculations. *J. Comput. Chem.* **1998**, *19*, 1746-1757.
94. Helgaker, T.; Klopper, W.; Koch, H.; Noga, J., Basis-set convergence of correlated calculations on water. *J. Chem. Phys.* **1997**, *106*, 9639-9646.
95. Feller, D., Application of systematic sequences of wave functions to the water dimer. *J. Chem. Phys.* **1992**, *96*, 6104-6114.
96. Weigend, F.; Häser, M.; Patzelt, H.; Ahlrichs, R., RI-MP2: optimized auxiliary basis sets and demonstration of efficiency. *Chem. Phys. Lett.* **1998**, *294*, 143-152.
97. Weigend, F., Accurate Coulomb-fitting basis sets for H to Rn. *Phys. Chem. Chem. Phys.* **2006**, *8*, 1057-1065.
98. Weigend, F.; Ahlrichs, R., Balanced basis sets of split valence, triple zeta valence and quadruple zeta valence quality for H to Rn: Design and assessment of accuracy. *Phys. Chem. Chem. Phys.* **2005**, *7*, 3297-3305.
99. Janssen, C. L.; Nielsen, I. M., New diagnostics for coupled-cluster and Møller-Plesset perturbation theory. *Chem. Phys. Lett.* **1998**, *290*, 423-430.
100. Jiang, W.; DeYonker, N. J.; Wilson, A. K., Multireference character for 3d transition-metal-containing molecules. *J. Chem. Theory Comput.* **2012**, *8*, 460-468.
101. Perdew, J. P.; Ruzsinszky, A.; Csonka, G. I.; Vydrov, O. A.; Scuseria, G. E.; Constantin, L. A.; Zhou, X.; Burke, K., Restoring the density-gradient expansion for exchange in solids and surfaces. *Phys. Rev. Lett.* **2008**, *100*, 136406.
102. Perdew, J. P.; Ruzsinszky, A.; Csonka, G. I.; Vydrov, O. A.; Scuseria, G. E.; Constantin, L. A.; Zhou, X.; Burke, K., Erratum: Restoring the Density-Gradient Expansion for Exchange in Solids and Surfaces [Phys. Rev. Lett. 100, 136406 (2008)]. *Phys. Rev. Lett.* **2009**, *102*, 039902.
103. Perdew, J. P.; Burke, K.; Ernzerhof, M., Generalized gradient approximation made simple. *Phys. Rev. Lett.* **1996**, *77*, 3865.
104. Perdew, J. P.; Burke, K.; Ernzerhof, M., Generalized Gradient Approximation Made Simple [Phys. Rev. Lett. 77, 3865 (1996)]. *Phys. Rev. Lett.* **1997**, *78*, 1396-1396.
105. Grimme, S.; Antony, J.; Ehrlich, S.; Krieg, H., A consistent and accurate ab initio parametrization of density functional dispersion correction (DFT-D) for the 94 elements H-Pu. *J. Chem. Phys.* **2010**, *132*, 154104.
106. Eichkorn, K.; Treutler, O.; Oehm, H.; Häser, M.; Ahlrichs, R., Auxiliary basis sets to approximate Coulomb potentials (Chem. Phys. Letters 240 (1995) 283-290). *CP* **1995**, *242*, 652-660.
107. Zhao, Y.; Truhlar, D. G., The Mo6 suite of density functionals for main group thermochemistry, thermochemical kinetics, noncovalent interactions, excited states, and transition elements: two new functionals and systematic testing of four Mo6-class functionals and 12 other functionals. *Theor. Chem. Acc.* **2008**, *120*, 215-241.

NO_x SCR in Cu-SSZ-13



TOC Graphic